Volume 28
Number 4
April 2026
Pages 869–1164

Environmental Science
Processes & Impacts

rsc.li/espi

ISSN 2050-7887

ROYAL SOCIETY OF CHEMISTRY

COMMUNICATION
Elijah G. Schnitzler *et al.*
Geranyl ester components of volatile chemical products readily induce black carbon restructuring

Environmental Science Processes & Impacts

ROYAL SOCIETY OF CHEMISTRY

COMMUNICATION

View Article Online
View Journal | View Issue

Cite this: *Environ. Sci.: Processes Impacts*, 2026, **28**, 925

Received 17th September 2025
Accepted 20th February 2026

DOI: 10.1039/d5em00761e

rsc.li/espi

Geranyl ester components of volatile chemical products readily induce black carbon restructuring

Christian A. Escritt, Habeeb H. Al-Mashala and Elijah G. Schnitzler *

Volatile chemical products (VCPs) are an emerging contaminant in the urban environment. Black carbon (BC) aggregates, initially highly branched, are also a prominent pollutant in the urban environment, emitted by diesel engines and other combustion sources outside and indoors, and they have effects on climate and public health that are influenced by their physical properties, *e.g.*, size and morphology. Here, we investigate the effects of geranyl esters, abundant components of fragrances in VCPs, on the morphology of laboratory generated BC aggregates. BC with an initial mobility diameter of 200 nm, generated by an inverted diffusion burner, was selected using a differential mobility analyzer (DMA) for coating experiments. We find that geranyl formate, acetate, propionate, and butyrate are extremely efficient at inducing BC restructuring. Complete compaction to a diameter growth factor of less than 0.75 occurs already at a volume growth factor as little as 1.01, *i.e.*, when the coating volume is 1% of the initial BC volume, in contrast to dioctyl sebacate, a common coating taken as a reference material. Compaction was also observed by scanning electron microscopy. Using a publicly available model of condensation to BC, we rationalize that this efficient restructuring occurs because the geranyl esters partition exclusively to point contacts between primary particles of BC through capillary condensation. Our results highlight the potential interactions of BC and VCPs, particularly in the indoor environment, where, *e.g.*, scented candles co-emit BC and fragrances.

Environmental significance

Black carbon (BC), a major component of particulate matter in urban environments, plays a significant role in climate and public health. In recent years, volatile chemical products (VCPs) have been recognized as a large source of indoor and urban air pollution, in both the gas and particle phases. Here, we show that geranyl esters, which are major components of many commercial fragrances in VCPs (*e.g.*, scented candles), are extremely efficient at restructuring BC aggregates, requiring a coating volume as little as 1% of the initial BC volume for maximum compaction. The size and morphology of BC govern to what extent it deposits in the respiratory system, so these interactions may play a role in the effects of BC on public health.

1. Introduction

Volatile chemical products (VCPs) are an emerging contaminant in the indoor and urban environment. While the use of major petrochemicals is largely dominated by natural gas and gasoline fuel, the small amount used for VCPs contributes a large fraction of the total mass of volatile organic compounds (VOCs) emitted from petrochemicals.[1] VCPs also have a significant potential to form secondary organic aerosol (SOA), potentially constituting nearly half of all SOA formed from petrochemicals, which can have further implications for air quality.[1] These VCPs are widely used in household products, and it is estimated that more than half of VCP emissions occur indoors.[4] These have a large impact on indoor air quality, as the confined space and limited airflow are key factors that allow them to reach elevated concentrations and persist indoors.[5,6] Eventually, after emission, much of the VCP mass from indoors passes into the outdoor urban environment, where the components can interact with oxidants to contribute to criteria pollutants, including fine particulate matter and ozone.[7]

Geranyl esters are major components of essential oils and widespread in VCPs. Geranyl acetate, shown in Fig. 1, constitutes up to 60% of eucalyptus oil,[8] and it has been detected in ambient air in a forest of Scots pine, *i.e.*, *Pinus sylvestris*.[9] These compounds are widely used as fragrances, *e.g.*, in reconstituted essential oils, personal care products, and scented candles.[10] Geranyl acetate, specifically, has been detected as an emission of commercial products used indoors, including diffusers, potpourri, and spray fragrances.[11] In passing, we note that geranyl acetate has also been tested for use as a repellent of pest species.[12,13] Because of their wide applications, geranyl esters are value-added chemicals, targets in a wide range of recent biosynthetic methods.[14–17]

Black carbon (BC) is another abundant pollutant in the urban environment, emitted largely from transportation.[18–20] BC

Department of Chemistry, Oklahoma State University, Stillwater, OK 74078, USA. E-mail: elijah.schnitzler@okstate.edu

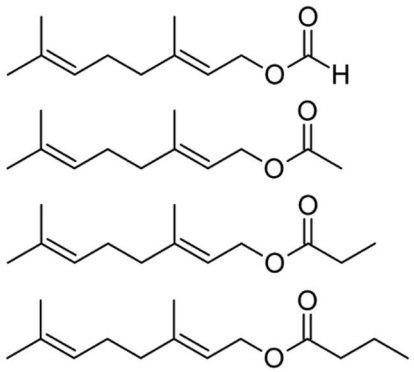

Fig. 1 Homologous series of geranyl esters: from top to bottom, geranyl formate, geranyl acetate, geranyl propionate, and geranyl butyrate.

alters the radiative balance of the atmosphere directly, by strongly absorbing solar radiation and decreasing surface albedo,[21] and indirectly, by influencing cloud properties.[22] BC also has significant effects on public health, and it has been found to be a factor in millions of deaths each year.[23] The extent of deposition of BC in the lungs is related to its shape and size.[24–26] BC aggregates are emitted initially as branched, fractal-like clusters of many smaller primary spherical particles.[27–29] Due to this initial morphology, BC can undergo restructuring to more compact morphologies upon coating during its residence time in the atmosphere.[30,31] Specifically, restructuring has been observed for coatings of water, sulfuric acid, and a variety of pure organic species,[32–38] in addition to complex mixtures, *e.g.*, SOA.[39–41] The efficacy of a given coating to induce restructuring is critical, as it determines the final morphology that in turn governs the effects of BC on climate and health.

Here, we probe the efficacy of geranyl esters, as representative components of VCPs, to induce BC restructuring. A homologous series of four geranyl esters was selected, from formate to butyrate (see Fig. 1), and compared to dioctyl sebacate, a reference species that has been used in previous studies.[35,36] BC aggregates were produced using a miniature inverted soot generator (MISG), and those with initial mobility diameters of 200 nm were selected using a differential mobility analyzer (DMA). These monodisperse particles were exposed to vapors of one of the geranyl esters or dioctyl sebacate in a saturator–condenser apparatus, and subsequent changes in mobility diameter for the BC aggregates were monitored using either a second DMA or an electrostatic particle classifier (EPC), coupled to a condensation particle counter (CPC). Imaging of particles before and after coating, collected with an electrostatic aerosol sampler (EAS), was also performed using scanning electron microscopy (SEM). Our results and their atmospheric implications are discussed below.

2. Materials and methods

2.1. Generation of black carbon

BC aggregates were generated using a setup that has been described in detail previously.[42] Briefly, BC was produced using a MISG (Argonaut, MISG-3) supplied with ethylene (Airgas, Ultra High Purity) and air (Airgas, Ultra Zero Grade) at flow rates of 0.1 and 10 L min^{-1}, respectively,[43,44] as shown in Fig. 2. From the exhaust of the burner, 0.3 L min^{-1} was directed through a denuder packed with activated carbon (Sigma-Aldrich, SBHL1410) followed by two denuders packed with silica gel desiccant (Parker, DRP-14-10B). The conditioned aerosol was then sent to an electrostatic classifier (TSI, 3082), equipped with a 0.0457 cm nozzle upstream of the inertial impactor, a soft X-ray advanced aerosol neutralizer (TSI, 3088), and a long DMA (TSI, 3081), with sample and sheath flow rates of 0.3 and 3 L min^{-1}, respectively. The DMA voltage was set to select particles with an electrical mobility diameter of 200 nm.

2.2. Coating of black carbon

The size-selected particles were then directed to the saturator–condenser apparatus (see Fig. 2). The saturator consisted of a glass bubbler in a sand bath on a hot plate, as described previously.[42] In each experiment, 200 μL of a particular coating compound was dispensed into the bottom of the bubbler using a calibrated micropipette. The stem of the bubbler was above the liquid level. The saturator temperature was increased incrementally for the duration of the experiment to increase the amount of coating material being applied to the BC aggregates.

Five pure liquid compounds were used as coating materials. Four were the following geranyl esters: geranyl formate (Sigma-Aldrich, >95%), geranyl acetate (Sigma-Aldrich, >97%), geranyl propionate (Sigma-Aldrich, >95%), and geranyl butyrate (Sigma-Aldrich, >95%). The fifth compound was dioctyl sebacate (Tokyo Chemical Industry, >98.0%). The vapor pressures of these compounds at room temperature (298.15 K) were estimated using predictions and, when available, experimental data at other temperatures. The methods of prediction used were the following: MPBPWIN (version 1.43), distributed in EPI Suite (version 4.1); SIMPOL.1, implemented in Excel;[45] SPARC, accessed online January 2025 (we note, in passing, that we can no longer access SPARC as of July 2025);[46] and ChemBCPP, accessed online July 2025.[47] For extrapolation from experimental data at other temperatures, we used the Antoine equation if the Antoine parameters were available.[48]

2.3. Characterization of particles upon coating

After coating in the saturator–condenser, the particles were directed alternately through one of two paths. In the first path, the sample was passed through a thermal denuder, described previously,[42,49] which was set to a temperature of 200 °C. In the second path, the sample was sent directly for characterization without passing through the thermal denuder. Two methods were used to characterize electrical mobility. In the first method, denoted Setup 1 (see Fig. 2), the sample was directed to a second DMA, which was equipped and operated the same as the first, followed by a CPC (TSI, 3750). The sample flow rate of the CPC is 1 L min^{-1}, but only 0.3 L min^{-1} was available from the conditioning and coating setup. The remaining 0.7 L min^{-1} was sampled from the laboratory through a particle filter. In the second method, denoted Setup 2 (see Fig. 2), the sample was

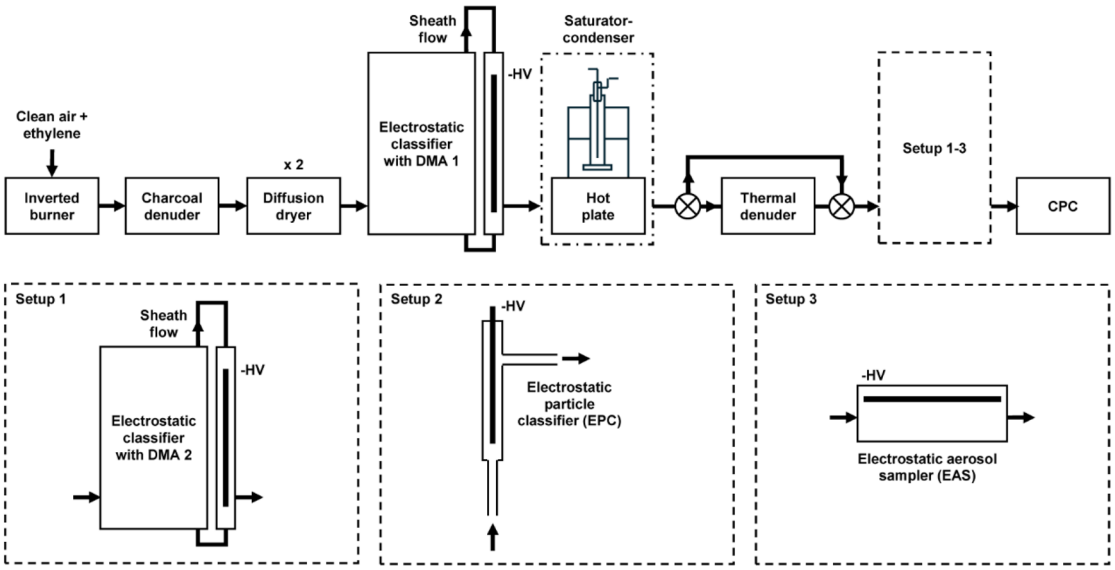

Fig. 2 Schematic of the experimental setup for the generation, coating, and characterization of BC aggregates. There were three setups in all, using either (1) the second DMA, (2) the EPC, or (3) the EAS, respectively. The three setups are not drawn to scale. DMA: differential mobility analyzer; CPC: condensation particle counter.

directed to an EPC, followed by the CPC. The EPC, illustrated in Fig. S1, was modelled after the design of Enekwizu *et al.*[50] The voltage was controlled using an external high-voltage power supply (Analog Technologies, AHVACN20KVR5MABT) and read using a multimeter. Details about the method and calibration are presented in Fig. S2 and S3. The bypass tubing was minimized to 4 cm in Setup 2 to characterize coated aggregates. The distribution of the coating on the BC aggregates was predicted using the online Capillary Condensation Model developed by the Khalizov group,[36,51–53] accessed July 2025.

2.4. Electron microscopy of black carbon

In addition to electrical mobility measurements, SEM was used to characterize the BC aggregates. To prepare samples of deposited BC for microscopy, we used Setup 3 (see Fig. 2), with a reconditioned EAS (TSI, 3100) where the second DMA or EPC was situated during electrical mobility measurements. The sample flow rate was the same, *i.e.*, 0.3 L min^{-1}. The precipitating voltage of the EAS was provided using the same power supply as was used for the EPC, set to −4.2 kV, as in past studies.[54,55] The corona discharge of the EAS was not used since the particles had already passed through an X-ray aerosol neutralizer in the first DMA. Silicon substrates (Ted Pella, 16006), 1 cm squares, were placed on the stage beneath the high voltage plate of the EAS, along the edge closest to the inlet. The sampler was run for 2 h to allow adequate deposition onto the silicon substrates. This sampling was completed for both uncoated-denuded aggregates and coated-denuded aggregates, to compare the initial and restructured BC. Imaging was performed on a scanning electron microscope (Thermo Fisher, FEI Quanta 600 FEG), operating at a voltage of 20 kV. The resulting images were analyzed using the Fiji distribution of ImageJ to determine the average diameter of the primary particles, based on 40 primary particles selected from four size-selected aggregates with a mobility diameter of 200 nm.[56–58]

3. Results and discussion

To begin, we performed our saturator–condenser experiments on a well characterized organic liquid, dioctyl sebacate, which has been used extensively as a proxy of organic aerosol.[59–62] More specifically, with an oxygen-to-carbon ratio of 0.15, dioctyl sebacate is a proxy of primary organic aerosol.[63] Furthermore, it has been used as a coating on BC aggregates from other sources and shown to induce restructuring.[35,36] A representative experiment with dioctyl sebacate on initially 200 nm BC aggregates from the miniature inverted burner is shown in Fig. 3a, in terms of mobility diameter as a function of saturator temperature. An initial mobility diameter of 200 nm was chosen because, first, it is larger than the peak of the polydisperse output (see Fig. S4) of the inverted burner (*i.e.*, minimizing the impact of multiply-charged particles) and, second, it is representative of the mean diameter of BC aggregates from transportation and biomass burning.[64] With Setup 1, the mobility diameters plotted in Fig. S5 are the geometric mean diameters of lognormal fits to number concentrations measured as the voltage of the second DMA was stepped (see Fig. S6). The geometric standard deviations of the fits were used to verify that the particles were monodisperse throughout each experiment.[65,66] With Setup 2, the mobility diameters plotted in Fig. 3 are based on the collection efficiencies measured with a fixed voltage (*i.e.*, 355 V) applied in the EPC (see Fig. S2).

Three stages are evident in the saturator–condenser experiment in Fig. 3a. The first stage began at the initial temperature, *i.e.*, room temperature. The initial mobility diameter of denuded particles, $d_{D,i}$ was the same as that of non-denuded

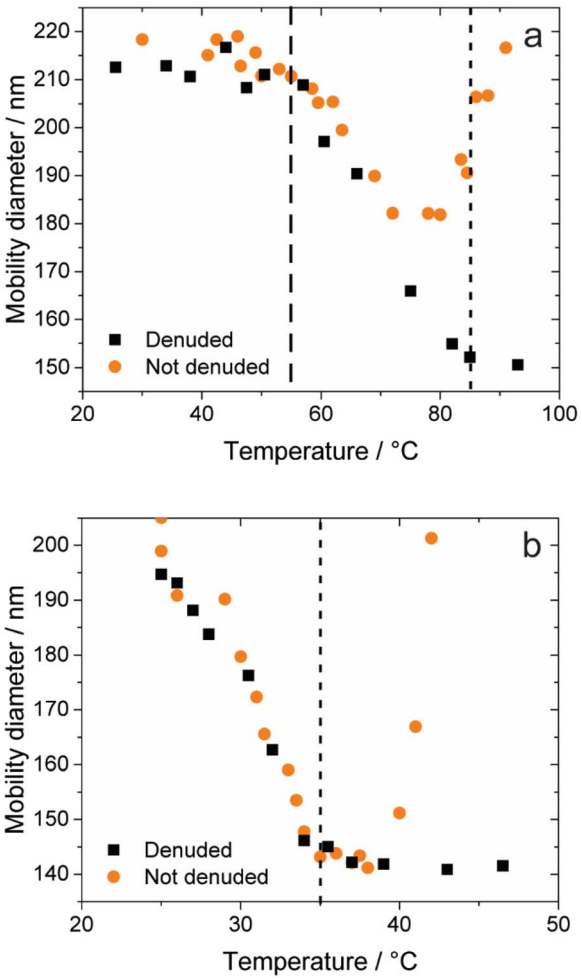

Fig. 3 Representative coating experiments using Setup 2 (*i.e.*, the EPC) with (a) dioctyl sebacate and (b) geranyl formate, showing evolution of the mobility diameter of particles with and without thermal denuding as a function of saturator temperature. The dashed line (a) denotes the onset of restructuring, *i.e.*, the second stage of the experiment. The dotted line (a and b) denotes near-complete restructuring of the coated BC aggregates. Note the different scales on the *x*-axes of the two panels.

particles, $d_{ND,i}$, since no coating was present. These mobility diameters were steady until the saturator temperature reached about 55 °C. At this temperature, marking the beginning of the second stage of the experiment, the mobility diameter of the denuded particles began decreasing due to the partitioning of dioctyl sebacate from the gas phase to the aggregates, downstream of the saturator, which induced restructuring of the BC cores. At the same time, the mobility diameter of the non-denuded (*i.e.*, coated) particles began decreasing like the denuded particles. This similarity indicates that appreciable restructuring occurs upon coating formation rather than removal, because the coating was intact on the non-denuded particles. As temperature increased further, the mobility diameter of the denuded particles decreased sigmoidally, reaching a plateau at about 85 °C, marking the end of the second stage. About halfway through this stage, at 70 °C, the mobility diameter of the non-denuded particles began increasing. This divergence of the denuded and non-denuded particles is due to the increasing coating volume required for further restructuring. At 85 °C, marking the beginning of the third stage of the experiment, the BC aggregates were fully restructured, with a final mobility diameter, $d_{D,f}$, of about 150 nm for the denuded particles. On the other hand, the coated particles continued to grow exponentially, as the gas-phase concentration of dioctyl sebacate increased with a temperature dependence described by the Clausius–Clapeyron equation. Heavily coated restructured BC aggregates are known to be spherical,[38] so the volume of coated particles during the final stage, $V_{ND,f}$ can be calculated geometrically from $d_{ND,f}$. Approximating the restructured BC cores as spheres is less precise but still reasonable,[38,67] so $V_{D,f}$ can be estimated similarly. These stages of restructuring have been observed in other coating experiments, including saturator–condenser experiments with pure liquids[68] as well as complex mixtures, *i.e.*, biomass burning organic aerosol (BBOA),[42] and smog chamber experiments with SOA.[39] Duplicate experiments for dioctyl sebacate with each of Setups 1 and 2 are shown in Fig. S7 and S8, respectively. From a comparison of results for non-denuded particles (see Fig. S9), it is evident that the DMA and EPC perform similarly for dioctyl sebacate. The similarity indicates that no evaporation of dioctyl sebacate occurred as the sample travelled from the condenser to the second DMA, consistent with previous measurements of low volatility coatings.[50]

A representative experiment with geranyl formate as the coating species is shown in Fig. 3b. From a comparison of the results for non-denuded particles (see Fig. S10), it is evident that evaporation of the geranyl esters occurred in Setup 1, upstream of the second DMA, consistent with previous observations of high volatility coatings.[50] Evaporation is prevented in Setup 2, as the EPC can be placed immediately (*i.e.*, 4 cm) downstream of the condenser. As in the above experiment with dioctyl sebacate, the mobility diameters of denuded and non-denuded particles changed significantly as a function of saturator temperature, which was increased from room temperature to about 50 °C. At room temperature, the initially 200 nm size-selected BC aggregates had already restructured slightly, and as the temperature increased, the mobility diameter decreased sharply, such that the aggregates were fully restructured at 35 °C. This transformation corresponds to the second stage of the experiment depicted in Fig. 3a. The onset of restructuring occurs at lower temperatures for geranyl formate than dioctyl sebacate. For comparisons here and below, vapor pressures at room temperature were estimated using several methods, as shown in Table 1. The estimates for a given species show good, *i.e.*, order-of-magnitude, agreement, except for the EPI Suite estimate for dioctyl sebacate. From the other estimates, the vapor pressure of dioctyl sebacate is many orders of magnitude (10^6 to 10^7) lower than that of the geranyl esters.

Throughout this entire stage of the experiment, the mobility diameters of the non-denuded (*i.e.*, coated) and denuded (*i.e.*, bare) particles overlapped closely. This observation supports two conclusions. First, the agreement indicates that restructuring occurs mostly during coating formation rather than removal, as inferred for dioctyl sebacate early in the second

Table 1 Estimated saturation vapor pressures of the geranyl esters and dioctyl sebacate at room temperature (298.15 K) using different methods of prediction

	Saturation vapor pressure (Pa)				
Method	Geranyl formate	Geranyl acetate	Geranyl propionate	Geranyl butyrate	Dioctyl sebacate
EPI suite	9.07×10^{0}	6.17×10^{0}	3.09×10^{0}	6.64×10^{-1}	2.62×10^{-4}
SIMPOL	6.01×10^{0}	2.26×10^{0}	8.51×10^{-1}	3.20×10^{-1}	2.79×10^{-7}
SPARC	8.62×10^{0}	2.43×10^{0}	9.68×10^{-1}	3.43×10^{-1}	1.44×10^{-7}
ChemBCPP	4.17×10^{0}	2.83×10^{0}	8.41×10^{-1}	2.72×10^{-1}	8.22×10^{-6}
Antoine	9.76×10^{0}	4.40×10^{0}	N/A[a]	4.65×10^{-1}	N/A[a]

[a] Antoine parameters not available for this compound.

stage depicted in Fig. 3a. Second, the extent of the agreement, *i.e.*, across this whole stage of restructuring, indicates that very little coating material is required for geranyl formate to fully restructure the BC aggregates, qualitatively less than for dioctyl sebacate, for which the data series diverge about halfway through the second stage (see Fig. 3a). Above 35 °C, the mobility diameter of coated-denuded particles reached a plateau, taken as $d_{D,f}$. The mobility diameter of the coated (*i.e.*, non-denuded) BC aggregates followed that of the denuded aggregates until the saturator exceeded 35 °C. Above 35 °C, the non-denuded aggregates began increasing in mobility diameter, exponentially. The exponential increase in diameter for the coated particles during this stage, as above, is consistent with fully restructured BC cores completely enveloped in spherical coatings of geranyl formate. Consistent observations were made for geranyl acetate, propionate, and butyrate. Duplicate experiments for the geranyl esters with each of Setups 1 and 2 are shown in Fig. S11–S18. The difference in morphology between the uncoated- and coated-denuded BC aggregates is evident from SEM images, in addition to electrical mobility measurements. As shown in Fig. 4, a representative BC aggregate before coating is highly branched, while a representative aggregate after coating with geranyl formate is compact, more closely approximated by a sphere; *i.e.*, branches have collapsed through coating and restructuring.

Note that there are differences between the duplicate experiments in terms of the non-denuded mobility diameters at elevated saturator temperatures, as the conditions governing the coating volume can vary between experiments; consequently, in the following discussion, the comparison between the geranyl esters and dioctyl sebacate will mostly be presented in terms of volume growth factor, the independent variable determining restructuring, as described below. During the last stage of the experiments, when the particles are assumed to be spherical, the volume of the coating, V_{coat}, is approximated by the difference between $V_{ND,f}$ and $V_{D,f}$. The resulting values of V_{coat} are fitted with an exponential function to interpolate between the initial (*i.e.*, zero) and final coating volumes to all saturator temperatures (see Fig. S19). The volume of the BC aggregates is the same throughout the experiment, *i.e.*, $V_{D,i} = V_{D,f}$, so the volume growth factor, Gfv, of the coated particles at any saturator temperature can be estimated by eqn (1) as follows:

$$\mathrm{Gfv} = \frac{V_{coat} + V_D}{V_D} \quad (1)$$

This approach to estimate Gfv has also been applied recently to discuss differences in BC restructuring induced by different volatility fractions of BBOA.[42] The diameter growth factor of the denuded BC aggregates is given by eqn (2):

$$\mathrm{Gfd} = \frac{d_{D,f}}{d_{D,i}} \quad (2)$$

where $d_{D,i}$ is the initial mobility of the aggregates with no coating (*i.e.*, 200 nm), and again $d_{D,f}$ is the mobility diameter of aggregates after coating and denuded, leading to smaller mobility diameters. When the diameter growth factor of the coated-denuded particles is plotted as a function of the volume growth factor of the coated particles, as shown in Fig. 5, the differences between the dioctyl sebacate and the geranyl ester coatings are further evident. The data series for the geranyl esters largely overlapped across the whole range of volume growth factors, exhibiting a sharp decrease to the final diameter growth factor when the volume growth factor was still close to one; the BC aggregates were fully restructured at a Gfv value as little as 1.01, *i.e.*, when the coating volume was only 1% of the BC volume. This is even less coating to induce complete restructuring than previously observed for fresh BBOA and is similar to that observed for high volatility compounds by Chen *et al.*[36,42] In contrast, the BC aggregates coated with dioctyl sebacate did not restructure at these small volume growth factors; these BC aggregates approached complete restructuring only at a Gfv value of about 2. This data series is similar to that

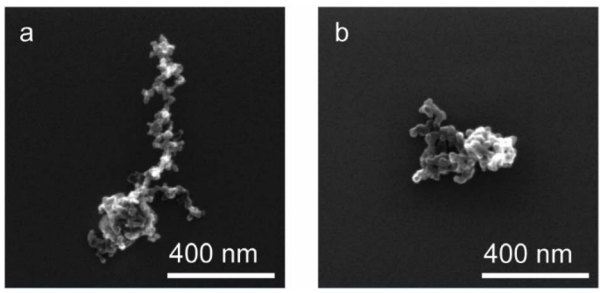

Fig. 4 SEM images of BC aggregates with an initial electrical mobility diameter of 200 nm (a) before and (b) after restructuring with geranyl formate.

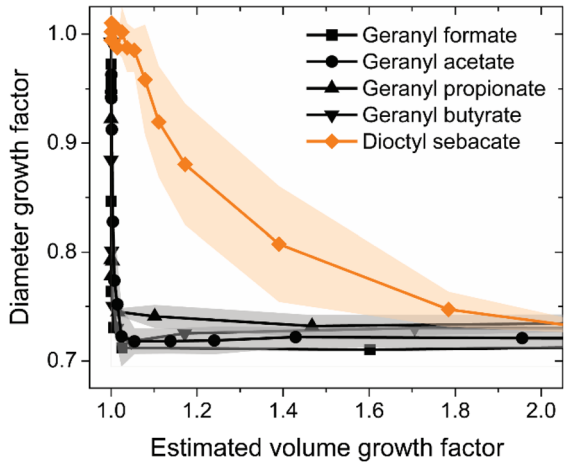

Fig. 5 Diameter growth factor of coated-denuded BC aggregates as a function of estimated volume growth factor of particles coated with a given geranyl ester or dioctyl sebacate. Replicate experiments were performed, and the shaded regions depict inter-experiment variance in terms of one standard deviation. The individual replicate experiments are shown in Fig. S8 for dioctyl sebacate and Fig. S15–S18 for the geranyl esters.

observed for highly evaporatively aged BBOA[42] as well as those observed for pure low volatility liquids.[36]

We discuss the differences between dioctyl sebacate and the geranyl esters in the context of the single-parameter model of BC aggregate restructuring developed by the Khalizov group.[36,51–53] The complex morphology of BC aggregates plays an important role in condensation.[36,52] On a primary particle of an aggregate, away from point contacts with its neighbours, the surface is convex, and condensation following adsorption may not occur even above the saturation vapor pressure, *i.e.*, due to the Kelvin effect.[69,70] At a point contact between primary particles, in contrast, the surface is concave, and condensation may occur even below the saturation vapor pressure, *i.e.*, capillary condensation.[52] A coating is most effective at inducing restructuring when its volume is distributed mostly near the point contacts rather than uniformly across the BC surface,[36,42] and a single parameter, χ, has been shown to describe this distribution of coating volume:

$$\chi = \frac{l_K}{R_s}\frac{1}{\zeta} \quad (3)$$

where l_K is the Kelvin length, R_s is the radius of the primary particles, and ζ is the reduced (*i.e.*, dimensionless) vapor supersaturation. When χ is about one or above, capillary rather than uniform condensation is favored.[36] Here, l_K for a given geranyl ester was calculated from its molar mass, density, and estimated surface tension. The surface tensions of the geranyl esters used are all in the range of 28.5–29.1 mN m^{-1} (see Table S1). From SEM image analysis of the BC aggregates produced here (see Fig. 4), the average diameter of the primary particles was found to be 25 ± 3 nm, so R_s was taken to be 12.5 nm.

To illustrate the distribution of volume, we focus here on geranyl butyrate. In the online Capillary Condensation Model, the rate of change in the coating volume, V_{coat}, through both capillary and uniform condensation, is expressed in eqn (4):[51,52]

$$\frac{dV_{coat}}{dt} = \frac{1}{4}A\alpha\omega\frac{Mp^o}{\rho RT}\left(S - \exp\left[\frac{1}{2}l_K\kappa\right]\right) \quad (4)$$

where t is time; A and κ are the area and mean curvature, respectively, of the vapor–liquid interface; α is the accommodation coefficient; R is the gas constant; T is temperature; and M, ρ, ω, l_K, p^o, and S are the molar mass, density, mean speed, Kelvin length, saturation vapor pressure, and vapor saturation, respectively, of the coating species. The rate at which a coating species reaches gas–particle partitioning equilibrium depends on its flux to the particle surface and, in turn, its number concentration in the gas phase. Even for the least volatile of the geranyl esters used here, with a saturated vapor pressure estimated from Antoine parameters to be 0.465 Pa (see Table 1), the gas number concentration at saturation or above is sufficient for the equilibrium capillary condensate volume to be reached extremely rapidly, *i.e.*, in less than 0.1 s, for a model aggregate of two primary particles with R_s of 12.5 nm, as implemented in the online Capillary Condensation Model.[71] The Kelvin length for geranyl butyrate is about 6 nm. The single parameter, χ, and equilibrium values of coating volume fraction, capillary condensate volume, and uniform condensate volume at (dimensionless) supersaturations from 1–0.001 are shown in Table S2. At the highest supersaturation, 1, the χ value is 0.47, much below one, and uniform condensation is highly favored. Reducing the supersaturation by an order of magnitude, to 0.1, increases the χ value proportionally, to give 4.7, indicating that now capillary condensation instead is highly favored; in fact, no uniform condensation is expected to occur. The total coating volume is significantly lower; the coating volume fraction is 0.234, corresponding to a Gfv of 1.31. Reducing ζ to 0.01 results in another order-of-magnitude increase in χ, further favoring capillary condensation. All the coating is again at the junction, but the volume is lower, such that Gfv is 1.11. Importantly, a further order-of-magnitude decrease in ζ has only a small effect on the capillary condensate volume, and Gfv is still about 1.11. Based on our electrical mobility measurements (see Fig. 5), this volume of coating is more than enough to induce complete restructuring of BC. Even when the gas-phase number concentration of geranyl butyrate is reduced below saturation, capillary condensation still occurs, due to the concave surface at the point contacts between primary particles. Consequently, under all but highly supersaturated conditions, geranyl butyrate will partition exclusively to the point contacts in BC, where liquid coatings are most effective at inducing restructuring. This is also the case for the other geranyl esters, which are more volatile than geranyl butyrate. These observations have implications regarding how VCPs and BC interact, as discussed below.

4. Atmospheric implications

Our results have implications for the interactions between VCPs and BC. In the indoor environment, the mean concentrations of the geranyl esters, like other fragrances,[5,72,73] will be low. For example, in samples collected in a house over 24 h for pre-

concentration on an adsorbent cartridge, the mass concentration of geranyl acetate was found to 18 ng m^{-3}.[74] At these gas-phase concentrations, no condensate is predicted to form in the simulations, even by capillary condensation. In real-time, gas-phase concentrations of fragrances can vary widely,[75] depending on emission sources, as well as room volume and air exchange rate; specifically, at a fixed emission rate, concentration can increase by orders of magnitude as room volume and air exchange rate decrease.[5] Moreover, geranyl esters, as major components of common essential oils, are used in scented candles, which are a source of co-emitted BC and VCPs. Except when they are smoldering, candles emit carbonaceous aerosol that is dominated by elemental carbon (*i.e.*, graphitic black carbon) rather than organic carbon (*i.e.*, functionalized organic compounds).[76] The comparatively bare BC from candles is similar in this regard to BC from diesel engines,[18,77,78] and BC from candles has been shown to similarly undergo significant restructuring upon coating, an indication of its initially highly branched morphology.[37] The elevated temperature of a burning candle could contribute to further increased saturation ratios near the source but away from the flame. Consequently, it is plausible that capillary condensation of geranyl esters and other fragrance components could occur, and together these species may induce restructuring, since only a miniscule coating volume is necessary. The morphology of candle BC plays an important role in deposition in the respiratory tract.[76] In the past, when BC from unscented candles was shown to have larger mobility diameters than BC from diesel engines, a lower probability of deposition was inferred.[76] If co-emitted VCPs undergo even minute capillary condensation onto candle BC, restructuring could lead to significantly lower mobility diameters, as shown here, and higher deposition probabilities. Finally, fragrances and other components of VCPs have recently been shown to form SOA upon oxidation in the atmosphere.[2,3,79,80] Since SOA from well-known biogenic and anthropogenic precursors has been shown to restructure BC upon gas–particle partitioning,[39,41] the interactions of BC and the oxidation products of fragrance components may also be relevant.

Conflicts of interest

There are no conflicts to declare.

Data availability

Data for this article, including the figures in the main text and supplementary information (SI), are available on zenodo at https://doi.org/10.5281/zenodo.17138373. Supplementary information is available. See DOI: https://doi.org/10.1039/d5em00761e.

Acknowledgements

The authors thank Brent Johnson and Lisa Whitworth for microscopy support and Ed Wright, Wes Cash, and Larry Vaughn for technical and fabrication support. They also thank Egor Demidov and Alexei Khalizov (New Jersey Institute of Technology) for helpful correspondence on their online simulator based on the single-parameter model, Nicholas Materer (Oklahoma State University) for helpful discussions on high-voltage electronics, and two anonymous reviewers for their helpful comments. This research was funded by the National Science Foundation through Grant AGS-2339449.

References

1 B. C. McDonald, J. A. de Gouw, J. B. Gilman, S. H. Jathar, A. Akherati, C. D. Cappa, J. L. Jimenez, J. Lee-Taylor, P. L. Hayes, S. A. McKeen, Y. Y. Cui, S.-W. Kim, D. R. Gentner, G. Isaacman-VanWertz, A. H. Goldstein, R. A. Harley, G. J. Frost, J. M. Roberts, T. B. Ryerson and M. Trainer, Volatile chemical products emerging as largest petrochemical source of urban organic emissions, *Science*, 2018, **359**, 760–764.
2 E. A. Pennington, K. M. Seltzer, B. N. Murphy, M. Qin, J. H. Seinfeld and H. O. T. Pye, Modeling secondary organic aerosol formation from volatile chemical products, *Atmos. Chem. Phys.*, 2021, **21**, 18247–18261.
3 S. Sasidharan, Y. He, A. Akherati, Q. Li, W. Li, D. Cocker, B. C. McDonald, M. M. Coggon, K. M. Seltzer, H. O. T. Pye, J. R. Pierce and S. H. Jathar, Secondary Organic Aerosol Formation from Volatile Chemical Product Emissions: Model Parameters and Contributions to Anthropogenic Aerosol, *Environ. Sci. Technol.*, 2023, **57**, 11891–11902.
4 A. Askari and A. W. H. Chan, Organic Emissions of Volatile Chemical Products in Canada: Emission Inventories, Indoor-to-Outdoor Transfer, and Regional Impacts, *Environ. Sci. Technol.*, 2024, **58**, 11074–11083.
5 T. Warburton, A. C. Lewis, J. R. Hopkins, S. J. Andrews, A. M. Yeoman, N. Owen, C. Jordan, G. Adamson and B. Xia, An assessment of VOC emissions and human strength perception of liquid electric fragrance diffusers, *Environ. Sci.: Adv.*, 2025, **4**, 739–752.
6 G. I. Gkatzelis, M. M. Coggon, B. C. McDonald, J. Peischl, K. C. Aikin, J. B. Gilman, M. Trainer and C. Warneke, Identifying Volatile Chemical Product Tracer Compounds in U.S. Cities, *Environ. Sci. Technol.*, 2021, **55**, 188–199.
7 K. M. Seltzer, B. N. Murphy, E. A. Pennington, C. Allen, K. Talgo and H. O. T. Pye, Volatile Chemical Product Enhancements to Criteria Pollutants in the United States, *Environ. Sci. Technol.*, 2022, **56**, 6905–6913.
8 K. Bauer, D. Garbe and H. Surburg, *Common Fragrance and Flavor Materials: Preparation, Properties and Uses*, John Wiley & Sons, 2008.
9 T. Dudek, M. Marć and B. Zabiegała, Chemical Composition of Atmospheric Air in Nemoral Scots Pine Forests and Submountainous Beech Forests: The Potential Region for the Introduction of Forest Therapy, *Int. J. Environ. Res. Public Health*, 2022, **19**, 15838.
10 D. L. J. Opdyke, Fragrance raw materials monographs: Geranyl acetate, *Food Cosmet. Toxicol.*, 1974, **12**, 885–886.
11 E. Uhde and N. Schulz, Impact of room fragrance products on indoor air quality, *Atmos. Environ.*, 2015, **106**, 492–502.

12 H. W. Kwon, S.-I. Kim, K.-S. Chang, J. M. Clark and Y.-J. Ahn, Enhanced Repellency of Binary Mixtures of Zanthoxylum armatum Seed Oil, Vanillin, and Their Aerosols to Mosquitoes Under Laboratory and Field Conditions, *J. Med. Entomol.*, 2011, **48**, 61–66.
13 L. Clark and J. Shivik, Aerosolized essential oils and individual natural product compounds as brown treesnake repellents, *Pest Manage. Sci.*, 2002, **58**, 775–783.
14 N. U. Haq, M. Liaquat, H. F. Alharby, Y. M. Alzahrani, S. A. Alghamdi, B. M. Alharbi, N. M. Alabdallah, S. Saud, M. Ahmed, R. Z. Sayyed and S. Fahad, Optimization and Purification of Terpenyl Flavor Esters Catalyzed by Black Cumin (Nigella sativa) Seedling Lipase in Organic Media, *Front. Sustainable Food Syst.*, 2022, **6**, 915602.
15 X. Wang, X. Zhang, J. Zhang, L. Xiao, Y. Zhou, Y. Zhang, F. Wang and X. Li, Genetic and Bioprocess Engineering for the Selective and High-Level Production of Geranyl Acetate in Escherichia coli, *ACS Sustainable Chem. Eng.*, 2022, **10**, 2881–2889.
16 T. Wu, S. Li, B. Zhang, C. Bi and X. Zhang, Engineering Saccharomyces cerevisiae for the production of the valuable monoterpene ester geranyl acetate, *Microb. Cell Factories*, 2018, **17**, 85.
17 S. Shukal, L. Ong, R. T, X. Chen and C. Zhang, Microaerobic Fermentation Enables High-Titer Biosynthesis of the Rose Monoterpenes Geraniol and Geranyl Acetate in Escherichia coli, *ACS Sustainable Chem. Eng.*, 2024, **12**, 3921–3932.
18 A. C. Eriksson, C. Wittbom, P. Roldin, M. Sporre, E. Öström, P. Nilsson, J. Martinsson, J. Rissler, E. Z. Nordin, B. Svenningsson, J. Pagels and E. Swietlicki, Diesel soot aging in urban plumes within hours under cold dark and humid conditions, *Sci. Rep.*, 2017, **7**, 12364.
19 M. Zavala, L. T. Molina, T. I. Yacovitch, E. C. Fortner, J. R. Roscioli, C. Floerchinger, S. C. Herndon, C. E. Kolb, W. B. Knighton, V. H. Paramo, S. Zirath, J. A. Mejía and A. Jazcilevich, Emission factors of black carbon and co-pollutants from diesel vehicles in Mexico City, *Atmos. Chem. Phys.*, 2017, **17**, 15293–15305.
20 S. Takahama, L. M. Russell, C. A. Shores, L. C. Marr, J. Zheng, M. Levy, R. Zhang, E. Castillo, J. G. Rodriguez-Ventura, P. J. E. Quintana, R. Subramanian, M. Zavala and L. T. Molina, Diesel vehicle and urban burning contributions to black carbon concentrations and size distributions in Tijuana, Mexico, during the Cal-Mex 2010 campaign, *Atmos. Environ.*, 2014, **88**, 341–352.
21 V. Ramanathan and G. Carmichael, Global and regional climate changes due to black carbon, *Nat. Geosci.*, 2008, **1**, 221–227.
22 C. C. Chuang, J. E. Penner, J. M. Prospero, K. E. Grant, G. H. Rau and K. Kawamoto, Cloud susceptibility and the first aerosol indirect forcing: Sensitivity to black carbon and aerosol concentrations, *J. Geophys. Res.: Atmos.*, 2002, **107**, AAC10.
23 J. Yang, M. J. Z. Sakhvidi, K. de Hoogh, D. Vienneau, J. Siemiatyck, M. Zins, M. Goldberg, J. Chen, E. Lequy and B. Jacquemin, Long-term exposure to black carbon and mortality: A 28-year follow-up of the GAZEL cohort, *Environ. Int.*, 2021, **157**, 106805.
24 L. Nicolaou, M. Fandiño-Del-Rio, K. Koehler and W. Checkley, Size distribution and lung-deposited doses of particulate matter from household exposure to biomass smoke, *Indoor Air*, 2021, **31**, 51–62.
25 T. J. Johnson, J. S. Olfert, C. U. Yurteri, R. Cabot and J. McAughey, Hygroscopic effects on the mobility and mass of cigarette smoke particles, *J. Aerosol Sci.*, 2015, **86**, 69–78.
26 Z. Zhang, C. Kleinstreuer and S. Hyun, Size-change and deposition of conventional and composite cigarette smoke particles during inhalation in a subject-specific airway model, *J. Aerosol Sci.*, 2012, **46**, 34–52.
27 Y. Pang, Y. Wang, Z. Wang, Y. Zhang, L. Liu, S. Kong, F. Liu, Z. Shi and W. Li, Quantifying the Fractal Dimension and Morphology of Individual Atmospheric Soot Aggregates, *J. Geophys. Res.: Atmos.*, 2022, **127**, e2021JD036055.
28 Y. Pang, M. Chen, Y. Wang, X. Chen, X. Teng, S. Kong, Z. Zheng and W. Li, Morphology and Fractal Dimension of Size-Resolved Soot Particles Emitted From Combustion Sources, *J. Geophys. Res.: Atmos.*, 2023, **128**, e2022JD037711.
29 C. M. Sorensen, The Mobility of Fractal Aggregates: A Review, *Aerosol Sci. Technol.*, 2011, **45**, 765–779.
30 J. Peng, M. Hu, S. Guo, Z. Du, J. Zheng, D. Shang, M. L. Zamora, L. Zeng, M. Shao, Y.-S. Wu, J. Zheng, Y. Wang, C. R. Glen, D. R. Collins, M. J. Molina and R. Zhang, Markedly enhanced absorption and direct radiative forcing of black carbon under polluted urban environments, *Proc. Natl. Acad. Sci. U. S. A.*, 2016, **113**, 4266–4271.
31 J. Peng, M. Hu, S. Guo, Z. Du, D. Shang, J. Zheng, J. Zheng, L. Zeng, M. Shao, Y. Wu, D. Collins and R. Zhang, Ageing and hygroscopicity variation of black carbon particles in Beijing measured by a quasi-atmospheric aerosol evolution study (QUALITY) chamber, *Atmos. Chem. Phys.*, 2017, **17**, 10333–10348.
32 X. Ma, C. D. Zangmeister, J. Gigault, G. W. Mulholland and M. R. Zachariah, Soot aggregate restructuring during water processing, *J. Aerosol Sci.*, 2013, **66**, 209–219.
33 J. Pagels, A. F. Khalizov, P. H. McMurry and R. Y. Zhang, Processing of Soot by Controlled Sulphuric Acid and Water Condensation—Mass and Mobility Relationship, *Aerosol Sci. Technol.*, 2009, **43**, 629–640.
34 A. F. Khalizov, H. Xue, L. Wang, J. Zheng and R. Zhang, Enhanced Light Absorption and Scattering by Carbon Soot Aerosol Internally Mixed with Sulfuric Acid, *J. Phys. Chem. A*, 2009, **113**, 1066–1074.
35 R. Ghazi and J. S. Olfert, Coating Mass Dependence of Soot Aggregate Restructuring due to Coatings of Oleic Acid and Dioctyl Sebacate, *Aerosol Sci. Technol.*, 2013, **47**, 192–200.
36 C. Chen, O. Y. Enekwizu, X. Fan, C. D. Dobrzanski, E. V. Ivanova, Y. Ma, G. Y. Gor and A. F. Khalizov, Single Parameter for Predicting the Morphology of Atmospheric Black Carbon, *Environ. Sci. Technol.*, 2018, **52**, 14169–14179.
37 B. Miljevic, N. C. Surawski, T. Bostrom and Z. D. Ristovski, Restructuring of carbonaceous particles upon exposure to organic and water vapours, *J. Aerosol Sci.*, 2012, **47**, 48–57.

38 R. P. Bambha, M. A. Dansson, P. E. Schrader and H. A. Michelsen, Effects of volatile coatings and coating removal mechanisms on the morphology of graphitic soot, *Carbon*, 2013, **61**, 80–96.

39 E. G. Schnitzler, A. Dutt, A. M. Charbonneau, J. S. Olfert and W. Jäger, Soot Aggregate Restructuring Due to Coatings of Secondary Organic Aerosol Derived from Aromatic Precursors, *Environ. Sci. Technol.*, 2014, **48**, 14309–14316.

40 C. Qiu, A. F. Khalizov and R. Zhang, Soot Aging from OH-Initiated Oxidation of Toluene, *Environ. Sci. Technol.*, 2012, **46**, 9464–9472.

41 H. Saathoff, K.-H. Naumann, M. Schnaiter, W. Schöck, O. Möhler, U. Schurath, E. Weingartner, M. Gysel and U. Baltensperger, Coating of soot and $(NH_4)_2SO_4$ particles by ozonolysis products of α-pinene, *J. Aerosol Sci.*, 2003, **34**, 1297–1321.

42 C. A. Escritt, K. L. Betz, M. R. Miles and E. G. Schnitzler, Dependence of black carbon restructuring on the volatility of biomass burning organic aerosol coatings at the wildland–urban interface, *Environ. Sci.: Atmos.*, 2025, **5**, 879–888.

43 M. Kazemimanesh, A. Moallemi, K. Thomson, G. Smallwood, P. Lobo and J. S. Olfert, A novel miniature inverted-flame burner for the generation of soot nanoparticles, *Aerosol Sci. Technol.*, 2019, **53**, 184–195.

44 A. Moallemi, M. Kazemimanesh, J. C. Corbin, K. Thomson, G. Smallwood, J. S. Olfert and P. Lobo, Characterization of black carbon particles generated by a propane-fueled miniature inverted soot generator, *J. Aerosol Sci.*, 2019, **135**, 46–57.

45 J. F. Pankow and W. E. Asher, SIMPOL.1: a simple group contribution method for predicting vapor pressures and enthalpies of vaporization of multifunctional organic compounds, *Atmos. Chem. Phys.*, 2008, **8**, 2773–2796.

46 S. H. Hilal, S. W. Karickhoff and L. A. Carreira, Prediction of the Vapor Pressure Boiling Point, Heat of Vaporization and Diffusion Coefficient of Organic Compounds, *QSAR Comb. Sci.*, 2003, **22**, 565–574.

47 J. Dong, N.-N. Wang, K.-Y. Liu, M.-F. Zhu, Y.-H. Yun, W.-B. Zeng, A. F. Chen and D.-S. Cao, ChemBCPP: A freely available web server for calculating commonly used physicochemical properties, *Chemom. Intell. Lab. Syst.*, 2017, **171**, 65–73.

48 D. R. Stull, Vapor Pressure of Pure Substances. Organic and Inorganic Compounds, *Ind. Eng. Chem.*, 1947, **39**, 517–550.

49 H. H. Al-Mashala, K. L. Betz, C. T. Calvert, J. A. Barton, E. E. Bruce and E. G. Schnitzler, Ultraviolet Irradiation Can Increase the Light Absorption and Viscosity of Primary Brown Carbon from Biomass Burning, *ACS Earth Space Chem.*, 2023, **7**, 1882–1889.

50 O. Y. Enekwizu, A. Hasani and A. F. Khalizov, Vapor Condensation and Coating Evaporation Are Both Responsible for Soot Aggregate Restructuring, *Environ. Sci. Technol.*, 2021, **55**, 8622–8630.

51 E. V. Demidov, G. Y. Gor and A. F. Khalizov, Discrete element method model of soot aggregates, *Phys. Rev. E*, 2024, **110**, 054902.

52 A. F. Khalizov, E. V. Ivanova, E. V. Demidov, A. Hasani, J. H. Curtis, N. Riemer and G. Y. Gor, Capillary Condensation: An Unaccounted Pathway for Rapid Aging of Atmospheric Soot, *Environ. Sci. Technol.*, 2025, **59**, 14564–14571.

53 E. V. Ivanova, A. F. Khalizov and G. Y. Gor, Kinetic model for competitive condensation of vapor between concave and convex surfaces in a soot aggregate, *Aerosol Sci. Technol.*, 2020, **55**, 302–315.

54 G. Mainelis, Collection of Airborne Microorganisms by Electrostatic Precipitation, *Aerosol Sci. Technol.*, 1999, **30**, 127–144.

55 B. Y. H. Liu, K. T. Whitby and H. H. S. Yu, Electrostatic Aerosol Sampler for Light and Electron Microscopy, *Rev. Sci. Instrum.*, 1967, **38**, 100–102.

56 J. Schindelin, I. Arganda-Carreras, E. Frise, V. Kaynig, M. Longair, T. Pietzsch, S. Preibisch, C. Rueden, S. Saalfeld, B. Schmid, J.-Y. Tinevez, D. J. White, V. Hartenstein, K. Eliceiri, P. Tomancak and A. Cardona, Fiji: an open-source platform for biological-image analysis, *Nat. Methods*, 2012, **9**, 676–682.

57 C. T. Rueden, J. Schindelin, M. C. Hiner, B. E. DeZonia, A. E. Walter, E. T. Arena and K. W. Eliceiri, ImageJ2: ImageJ for the next generation of scientific image data, *BMC Bioinf.*, 2017, **18**, 529.

58 C. A. Schneider, W. S. Rasband and K. W. Eliceiri, NIH Image to ImageJ: 25 years of image analysis, *Nat. Methods*, 2012, **9**, 671–675.

59 I. J. George, A. Vlasenko, J. G. Slowik, K. Broekhuizen and J. P. D. Abbatt, Heterogeneous oxidation of saturated organic aerosols by hydroxyl radicals: uptake kinetics, condensed-phase products, and particle size change, *Atmos. Chem. Phys.*, 2007, **7**, 4187–4201.

60 S. Jain and G. A. Petrucci, A New Method to Measure Aerosol Particle Bounce Using a Cascade Electrical Low Pressure Impactor, *Aerosol Sci. Technol.*, 2015, **49**, 390–399.

61 J. D. Hearn, L. H. Renbaum, X. Wang and G. D. Smith, Kinetics and products from reaction of Cl radicals with dioctyl sebacate (DOS) particles in O_2: a model for radical-initiated oxidation of organic aerosols, *Phys. Chem. Chem. Phys.*, 2007, **9**, 4803–4813.

62 J. C. Corbin, D. Clavel and G. J. Smallwood, Characterization of two aerosol carbon analyzers based on temperature programmed oxidation: TCA08 and FATCAT, *Aerosol Sci. Technol.*, 2024, **58**, 812–829.

63 F. Mahrt, E. Newman, Y. Huang, M. Ammann and A. K. Bertram, Phase Behavior of Hydrocarbon-like Primary Organic Aerosol and Secondary Organic Aerosol Proxies Based on Their Elemental Oxygen-to-Carbon Ratio, *Environ. Sci. Technol.*, 2021, **55**, 12202–12214.

64 P. Beeler, J. Kumar, J. P. Schwarz, K. Adachi, L. Fierce, A. E. Perring, J. M. Katich and R. K. Chakrabarty, Light absorption enhancement of black carbon in a pyrocumulonimbus cloud, *Nat. Commun.*, 2024, **15**, 6243.

65 M. Gysel, G. B. McFiggans and H. Coe, Inversion of tandem differential mobility analyser (TDMA) measurements, *J. Aerosol Sci.*, 2009, **40**, 134–151.

66 M. R. Stolzenburg and P. H. McMurry, Equations Governing Single and Tandem DMA Configurations and a New Lognormal Approximation to the Transfer Function, *Aerosol Sci. Technol.*, 2008, **42**, 421–432.
67 T. A. Sipkens and J. C. Corbin, Effective density and packing of compacted soot aggregates, *Carbon*, 2024, **226**, 119197.
68 E. G. Schnitzler, J. M. Gac and W. Jäger, Coating surface tension dependence of soot aggregate restructuring, *J. Aerosol Sci.*, 2017, **106**, 43–55.
69 A. Laaksonen, J. Malila and A. Nenes, Heterogeneous nucleation of water vapor on different types of black carbon particles, *Atmos. Chem. Phys.*, 2020, **20**, 13579–13589.
70 Y. Crouzet and W. H. Marlow, Calculations of the Equilibrium Vapor Pressure of Water over Adhering 50–200-nm Spheres, *Aerosol Sci. Technol.*, 1995, **22**, 43–59.
71 Capillary condensation model, https://www.edemidov.com/capillary-condensation/, accessed 3 September 2025.
72 W.-H. Cheng, D.-Y. Tsai, J.-Y. Lu and J.-W. Lee, Extracting Emissions from Air Fresheners Using Solid Phase Microextraction Devices, *Aerosol Air Qual. Res.*, 2016, **16**, 2362–2367.
73 W.-H. Cheng and C.-H. Lai, Sampling gaseous compounds from essential oils evaporation by solid phase microextraction devices, *Atmos. Environ.*, 2014, **99**, 124–129.
74 C. Balducci, M. Cerasa, P. Avino, P. Ceci, A. Bacaloni and M. Garofalo, Analytical Determination of Allergenic Fragrances in Indoor Air, *Separations*, 2022, **9**, 99.
75 T. Warburton, S. K. Grange, J. R. Hopkins, S. J. Andrews, A. C. Lewis, N. Owen, C. Jordan, G. Adamson and B. Xia, The impact of plug-in fragrance diffusers on residential indoor VOC concentrations, *Environ. Sci.: Processes Impacts*, 2023, **25**, 805–817.
76 J. Pagels, A. Wierzbicka, E. Nilsson, C. Isaxon, A. Dahl, A. Gudmundsson, E. Swietlicki and M. Bohgard, Chemical composition and mass emission factors of candle smoke particles, *J. Aerosol Sci.*, 2009, **40**, 193–208.
77 D. Li, J. Wei, H. Chen, C. Wang and C. Wang, Study on the restructuring of soot particles from diesel engine exhaust gas discharged into a simulated atmospheric environment, *Fuel*, 2023, **349**, 128679.
78 K. K. Leung, E. G. Schnitzler, R. Dastanpour, S. N. Rogak, W. Jäger and J. S. Olfert, Relationship between Coating-Induced Soot Aggregate Restructuring and Primary Particle Number, *Environ. Sci. Technol.*, 2017, **51**, 8376–8383.
79 A. A. Akande and N. Borduas-Dedekind, The gas phase ozonolysis and secondary OH production of cashmeran, a musk compound from fragrant volatile chemical products, *Environ. Sci.: Processes Impacts*, 2025, **27**, 1504–1516.
80 M. B. Humes, M. Wang, S. Kim, J. E. Machesky, D. R. Gentner, A. L. Robinson, N. M. Donahue and A. A. Presto, Limited Secondary Organic Aerosol Production from Acyclic Oxygenated Volatile Chemical Products, *Environ. Sci. Technol.*, 2022, **56**, 4806–4815.

